The diffracted magneto-optic Kerr effect: what does it tell you?

2004 J. Phys.: Condens. Matter 16 R275

(http://iopscience.iop.org/0953-8984/16/9/R01)

INSTITUTE OF PHYSICS PUBLISHING JOURNAL OF PHYSICS: CONDENSED MATTER

J. Phys.: Condens. Matter **16** (2004) R275–R294 PII: S0953-8984(04)60720-X

TOPICAL REVIEW

The diffracted magneto-optic Kerr effect: what does it tell you?

M Grimsditch[1] **and P Vavassori**[2]

[1] Materials Science Division, Argonne National Laboratory, Argonne, IL 60439, USA
[2] INFM—National Research Centre for Nanostructures and Biosystems at Surfaces, Dipartimento di Fisica, Universita di Ferrara, Italy

Received 3 November 2003
Published 20 February 2004
Online at stacks.iop.org/JPhysCM/16/R275 (DOI: 10.1088/0953-8984/16/9/R01)

Abstract

The experimental and theoretical aspects of obtaining the magnetic information carried by laser beams diffracted from an array of nanosized magnetic objects are reviewed. Experimentally it will be shown that the magneto-optic Kerr effect (MOKE) hysteresis loops recorded for diffracted beams can be quite different from those recorded for the reflected beam. We will show that the diffracted MOKE (D-MOKE) loops are proportional to the magnetic form factor or, equivalently, to the Fourier component of the magnetization corresponding to the reciprocal lattice vector of the diffracted beam. In conjunction with micromagnetic simulations, the D-MOKE provides a powerful and non-destructive technique for investigating the magnetization reversal process in submicron-sized magnetic particles. The advantages and disadvantages of the D-MOKE technique will be compared to those of other techniques that yield related information (e.g. magnetic force microscopy, Lorentz electron microscopy and micromagnetic simulations).

(Some figures in this article are in colour only in the electronic version)

Contents

1. Introduction

The magneto-optic Kerr effect (MOKE) technique is well established for the investigation of magnetic materials [1–3]. Relying on small, magnetization induced changes in the optical properties which in turn modify the polarization or the intensity of the reflected light, the technique has been used to measure the magnetic hysteresis loops of innumerable systems, usually in thin film form or *in situ*, where other techniques such as SQUID investigation are not as suitable. Unlike SQUID measurements, the MOKE technique seldom yields an absolute value for the magnetization; typically the hysteresis loops are normalized to unity at saturation.

As is well known for optical gratings, when a beam of light is incident upon a sample that has a structure comparable to the wavelength of the radiation, the beam is not only reflected but is also diffracted. If the material is magnetic, one may ask whether the diffracted beams also carry information about the magnetic structure. Experimentally this is an easy question to answer: figure 1 shows the D-MOKE hysteresis loops measured in various diffraction orders from an array of 800 nm circular Permalloy discs. Clearly these data indicate that there is magnetic information in the diffracted beams and that this information is not identical to that in the reflected beam. The purpose of this review is to describe the progress that has been made in the interpretation of these hysteresis loops.

First we will describe the experimental set-up that we have used as well as other possible experimental geometries. The theoretical formalism that we have developed to interpret the experimental data is presented in section 3. The fourth section briefly covers aspects of micromagnetic simulations that are relevant to our data analysis. In the results section we review examples from the literature where the D-MOKE technique has been used to understand the magnetization reversal path in patterned magnetic arrays. In the final section we summarize the type of information that can be extracted with the D-MOKE technique. We also compare the D-MOKE technique with other techniques that yield similar information, highlighting both advantages and disadvantages. One of the main conclusions is that the D-MOKE is a powerful tool for testing the validity of the many assumptions (e.g. subtle shape effects, growth induced anisotropies, direction of the applied field) that must be made in micromagnetic simulations.

2. Experimental details

We first remind the reader that there are three distinct geometries used for the conventional MOKE technique: polar, longitudinal and transverse. The first two are sensitive to the components of magnetization (M) perpendicular to the sample plane and to the in-plane component lying in the scattering plane, respectively. In both these geometries it is the polarization state of the reflected light which must be monitored. The transverse MOKE geometry is sensitive to the in-plane component of M that is perpendicular to the scattering plane. In this geometry the magnetic field induced changes also appear as intensity changes of the reflected light. There is no *a priori* reason that any one of these geometries should be more or less suitable for the D-MOKE technique. However, since the polar and longitudinal geometries depend on at least two Fresnel (reflectivity) coefficients while the transverse MOKE technique depends only on one (r_{pp}), the interpretation of the data is greatly simplified for the latter. For this reason all our published data have been recorded in the transverse MOKE configuration and we will restrict most of the discussion in this article to this geometry.

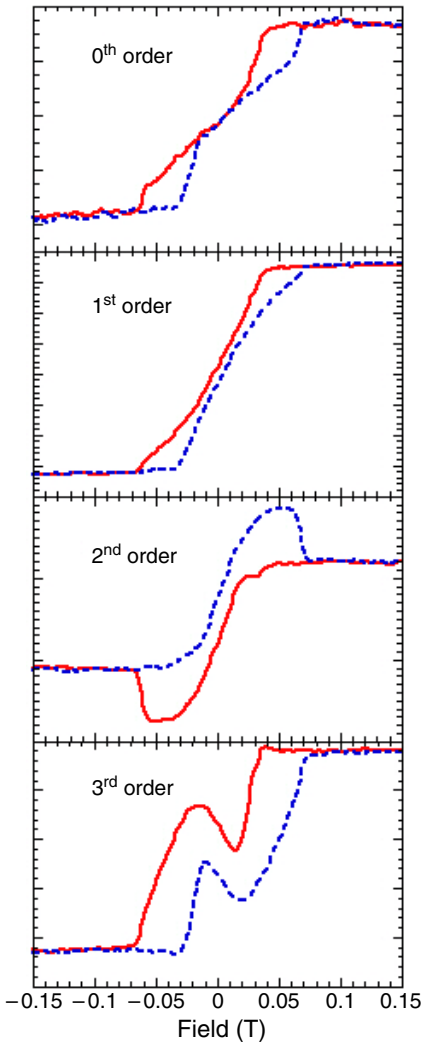

Figure 1. D-MOKE hysteresis loops from 800 nm Permalloy discs measured for various diffraction orders. The full and dashed curves are for decreasing and increasing field values respectively.

A block diagram of the transverse MOKE geometry is shown in figure 2. A suitably intensity-stabilized laser beam impinges on the patterned array sample placed between the poles of an electromagnet. This gives rise to the reflected and diffracted beams shown in the figure. In this Kerr geometry the magnetic field (H) can be applied either in the scattering plane (as shown in the figure) or perpendicular to it. In both cases the reflected light is sensitive to the component of M perpendicular to the scattering plane, so by varying the direction of H the components of M perpendicular and parallel to H can be measured. (These are typically called the transverse and longitudinal components of the magnetization; they must not be confused with the transverse and longitudinal Kerr geometries.) In principle the detector can be placed in any of the diffracted beams. However, for diffracted beams out of the scattering plane it is no longer clear which Kerr geometry—and consequently which component of M—should be used in the analysis. Since the theory for magnetic effects in diffracted beams out of the

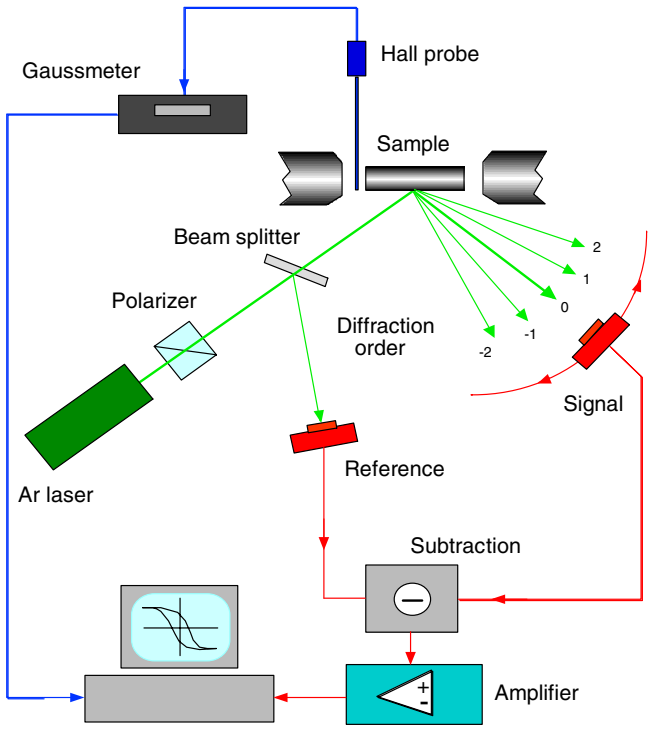

Figure 2. A block diagram of the set-up used for diffracted MOKE studies.

scattering plane has not yet been developed, we will restrict our analysis to diffracted beams in the scattering plane.

There are two options for reducing the noise in the detected beam. Shown in figure 2 is the use of a reference beam. The signals from the detector and reference beams are adjusted via load resistors so that they are equal. Their difference is then fed into a DC amplifier–filter whose output is fed into the data acquisition system together with the signal from the Hall probe. Our acquisition system generates a sawtooth output that drives the power supply to the magnet. An alternative option for noise reduction is the use of conventional lock-in techniques. The two systems yield similar results.

3. Theory

A rigorous theoretical solution to the D-MOKE problem requires the complete diffraction theory including the magneto-optical contributions. The latter contributions in turn require full knowledge of the magnetic configuration of the system. Such an approach yields the absolute intensities and the magnitudes of the magnetic contributions in each diffracted beam. In the vector diffraction approach, not only must the boundary conditions for all the diffracted waves be included but also the magneto-optic contributions in the material itself. The general solution must also account for the longitudinal, polar and transverse Kerr geometries. Various forms of this full formalism have been used to solve some magnetic diffraction problems [4–9]. These investigations have, in general, dealt with grating-like structures and have focused mainly on the magnitudes of the changes between the two saturated states. In a few instances the formalism has been applied to a few simple domain configurations of a grating.

A different approach, based more on a local radiating dipole picture, was presented in [10] and has many aspects in common with the formalism to be discussed here. The formalism that will be outlined below evolved out of a need for a physically more transparent description which, although not rigorous, still provides a basic understanding of aspects of magnetization reversal. The equations that will be postulated have resulted more from an analogy with other physical systems than from any detailed derivation. In [11, 12] very similar equations have also been independently proposed. Although these equations will be shown to lead to a convenient formalism with which to interpret the D-MOKE results, the equations should be treated with some caution since they may not be valid for all situations. We also forewarn the reader that with these equations we make no attempt to predict the intensity of the magneto-optic effects, but purport only to describe the behaviour of the intensity changes caused by changes in the magnetization configuration in each particle.

The conventional MOKE is described in terms of the Fresnel coefficients (r) which describe the ratio of the electric fields in the reflected and incident beams. TM polarized (p) and TE polarized (s) polarizations of the incident and reflected light define the ratios r_{pp}, r_{ss}, r_{ps} and r_{sp}. For the transverse Kerr geometry of an infinite, flat film the relevant reflectivity is

$$r_{\mathrm{pp}} + m_{\perp} r_{\mathrm{pp}}^{\mathrm{m}} \tag{1}$$

where r_{pp} and $r_{\mathrm{pp}}^{\mathrm{m}}$ are the non-magnetic and magnetic parts of the reflectivity, and $m_{\perp}$ is the average magnetization, normalized to the saturation value, perpendicular to the scattering plane over the illuminated area. In cases where m is a function of position it is shown that $m_{\perp}$ should be replaced by its spatial average $\langle m_{\perp} \rangle$.

For a patterned surface (ignoring the magnetic contributions) the physical optics approximation [13] (see equation (16) on p 4727) predicts that the electric field in the nth-order diffraction beam is proportional to the product of r_{pp} times the form factor f_n defined by

$$f_n = \int \exp\{\mathrm{i}nGr\}\,\mathrm{d}S, \tag{2}$$

where the integration is carried out over one unit cell of the array and G is the reciprocal lattice vector. (Equation (2) implicitly assumes that r_{pp} is independent of the position within each magnetic particle.) It must be noted however that r_{pp} itself also depends on the incidence and scattering angles. This dependence is typically quite weak (<60%) for opaque materials. If we forgo the comparison of the magnitude of the effect in different orders, taking r_{pp} as the same constant at all orders is usually a reasonable approximation. It should be noted that if the surface is not flat it will also be necessary to include the relevant phase changes due to the corrugation in equation (2).

On the basis of equations (1) and (2) it is reasonable to generalize the electric field in the nth-order diffracted beam from a magnetic patterned surface (E_n) via

$$E_n = E_0(r_{\mathrm{pp}} f_n + r_{\mathrm{pp}}^{\mathrm{m}} f_n^{\mathrm{m}}) \tag{3}$$

where E_0 is the incident electric field and f_n^{m} is defined by

$$f_n^{\mathrm{m}} = \int m_{\perp}(r) \exp\{\mathrm{i}nGr\}\,\mathrm{d}S. \tag{4}$$

Here again the caveat that $r_{\mathrm{pp}}^{\mathrm{m}}$ is also angle dependent must be noted. Furthermore, since its angular dependence will not be the same as that of r_{pp}, the ratio $r_{\mathrm{pp}}/r_{\mathrm{pp}}^{\mathrm{m}}$ in equation (3) must be considered as a number that may have a dependence on the diffracted order.

Since the intensity of the diffracted beam is given by EE^*, it follows from equation (3) that the magnetic contribution to the diffracted intensity (ΔI_n) can be cast in the form [14]

$$\Delta I_n \propto \mathrm{Re}[f_n^{\mathrm{m}}(r_{\mathrm{pp}}^{\mathrm{m}}/r_{\mathrm{pp}})] \propto \mathrm{Re}[f_n^{\mathrm{m}}] + A_n\,\mathrm{Im}[f_n^{\mathrm{m}}] \tag{5}$$

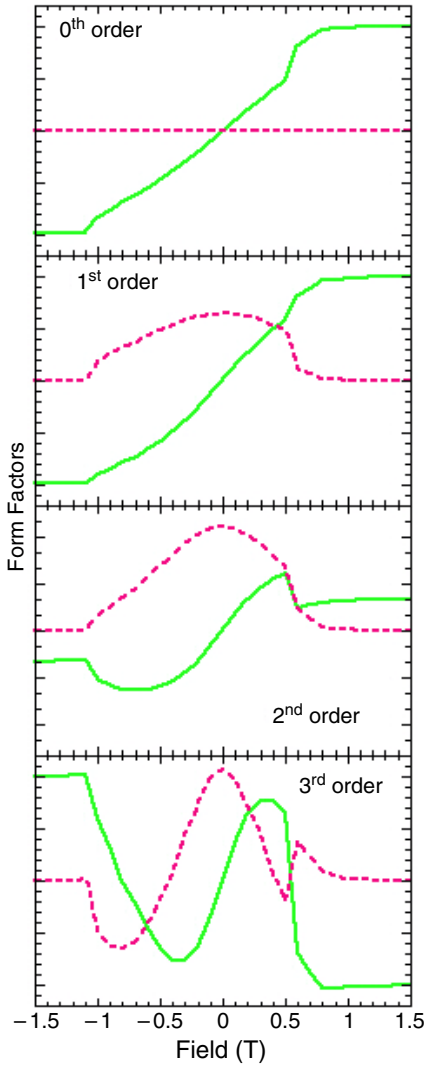

Figure 3. The field dependence of the magnetic form factors for Py discs whose measured loops are shown in figure 1, calculated using micromagnetic simulations. The full and dashed curves are the real and imaginary parts of the form factor.

where A_n is a number. In principle, A_n can be evaluated from r_{pp} and r_{pp}^{m}. However, this requires an accurate knowledge of all the optical constants of both substrate and particles, the magneto-optic coefficients, the thickness of the particles, and the angle of incidence. Also, implicit in equation (3), it assumes that the functional forms used for the Fresnel coefficients are independent of the diffraction angle. In the examples to be reviewed below, A_n has been treated as an adjustable parameter, so no attempt will be made to pursue this issue here. How it is adjusted will be described in section 5: *Vortices*. Note also that equation (5) provides no information on the magnitude of the magnetic signal; it only describes how the magnetic intensity changes as the magnetization configuration within each particle evolves.

It is clear from equation (5) that if the magnetic distribution within each particle were known as a function of field, it would be possible to calculate the D-MOKE loops of any order.

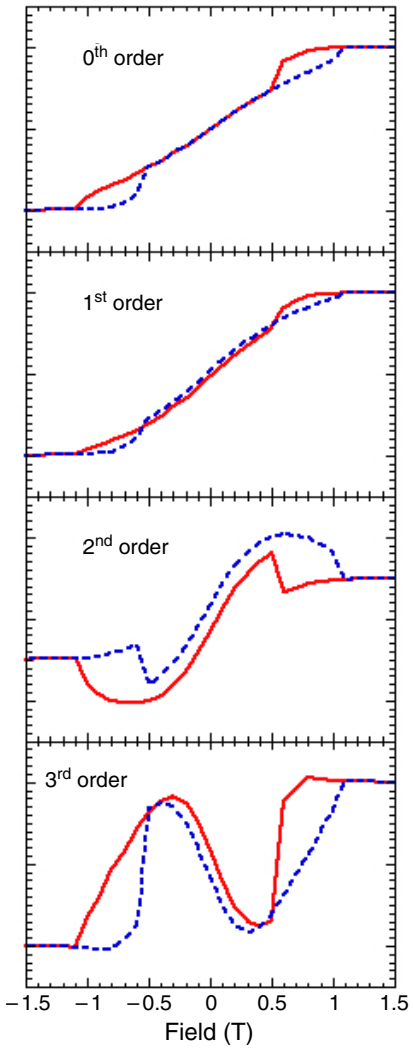

Figure 4. Hysteresis loops for Py discs calculated with the form factors in figure 3. The full and dashed curves are for decreasing and increasing field values respectively.

This is the exact equivalent to being able to calculate the intensity of any x-ray Bragg peak if the unit cell is known. The converse problem, i.e. extracting the unit cell from Bragg intensities or the magnetic configuration from the D-MOKE loops, is also conceptually identical. However, the relatively few diffracted orders in the case of the MOKE—compared to x-rays—do not yet allow the inverse solution to be found. In the absence of such solutions the D-MOKE data can only be used as a test of a proposed magnetic configuration. At first sight this limitation would appear to be so severe as to render the technique almost useless. It turns out however that the D-MOKE results, when used in conjunction with micromagnetic simulations, provide a powerful and unique tool for investigating magnetization in nanostructures.

4. Micromagnetic simulations

Micromagnetic simulations [15] are the magnetic equivalent of molecular dynamics simulations for structural studies. They solve the equations of motion for all the spins (or

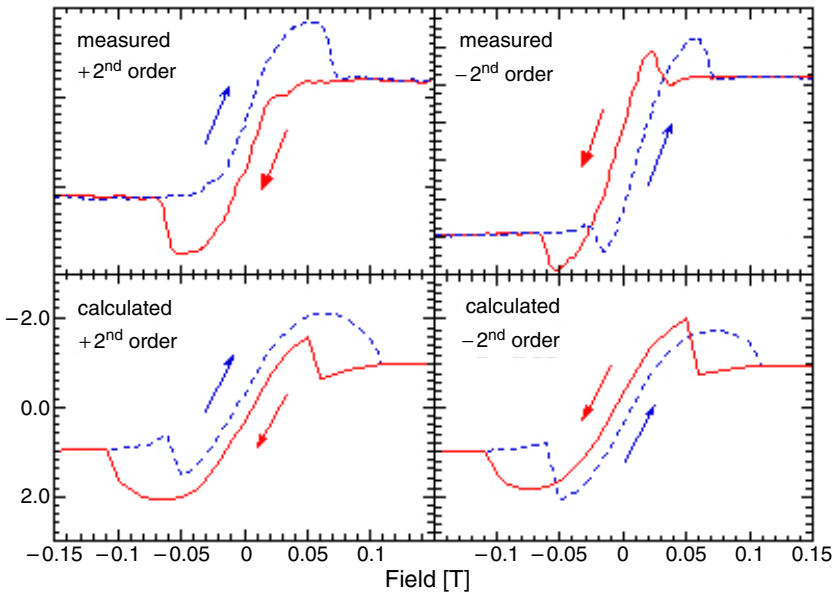

Figure 5. Measured (upper) and calculated (lower) ±second-order D-MOKE loops.

groups of spins) in a magnetic sample and find the configuration $m(r)$ for which the torque on all spins is zero. Typically, micromagnetic simulations require input of the material parameters (magnetization, exchange and anisotropies, damping), the particle shape and the applied field. The output ($m(r)$) of such calculations can be used to evaluate the magnetic form factors (equation (4)), and this can be done for a range of applied fields. With this information the D-MOKE hysteresis loops can then be calculated using equation (5).

At this point some readers may wonder, if the magnetic configurations in particles can be easily calculated using micromagnetics, why bother with the D-MOKE? The answer, as will become clear in the next section, is in cases where the micromagnetic simulations do not predict the observed D-MOKE loops. In these cases it is necessary to re-evaluate the assumptions that enter the micromagnetic simulations and determine whether, with some other combination of parameters, agreement can be obtained.

The simulations to be discussed in the next section were performed using the NIST OOMMF software [16]. For each system that was investigated the equilibrium magnetization configuration was calculated for 10–20 values of the applied field covering the range of magnetization reversal. The zeroth-order hysteresis loop, which corresponds to the average magnetization (see equation (4) with $n = 0$), is provided directly by the OOMMF program. The higher order diffraction loops require extracting the magnetization distribution from OOMMF, and performing the integration in equation (4) for the desired component of the magnetization (in the plane of the sample and perpendicular to the scattering plane for the case of the transverse Kerr geometry) and for all desired values of n. With the values of f_n thus obtained, the hysteresis loops are calculated with equation (5) using A_n as an adjustable parameter.

The issue of 'coupling' between neighbouring particles is a non-trivial problem for the micromagnetic simulations. For an array of well-spaced particles it can be argued that the coupling (dipolar) will be small and that micromagnetic simulations of a single particle are adequate. If the particles are in close proximity it is necessary to simulate an array of particles that is large enough that edge effects can be neglected. The form factors are then calculated

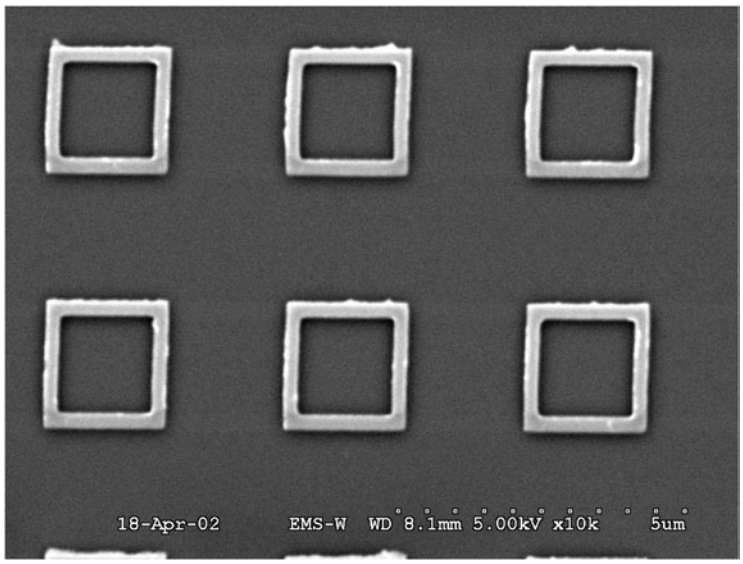

Figure 6. An SEM image of square Py rings.

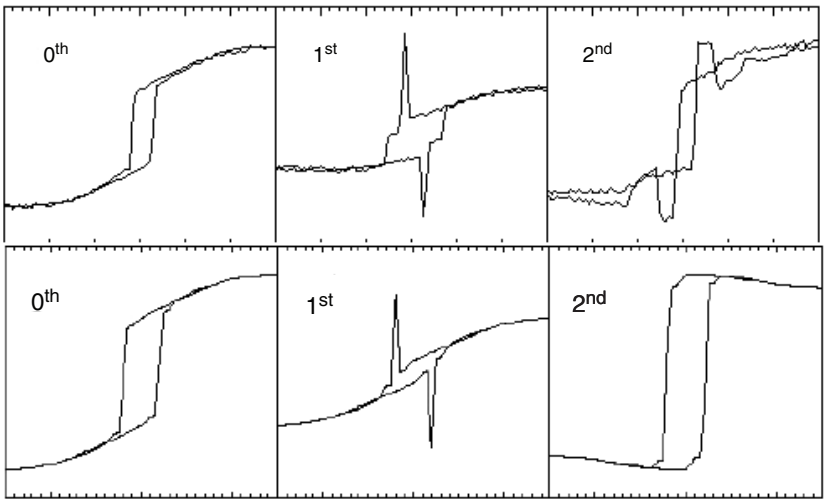

Figure 7. D-MOKE zeroth–second-order hysteresis loops for Py square rings with $H \parallel$ edge. The upper loops are experimental. The lower loops are calculated using micromagnetics from an asymmetric square ring.

for the central particle with the assumption that it is representative of a general element in an extended array. The problem is even more serious when dealing with negative arrays since in these cases not only is the coupling between neighbouring unit cells large but also the edge effects of the outer border of the simulation cell produce undesired effects. In these cases the edge effects can be reduced by making the edges of the simulation cell rough. However, even with this gambit, the number of unit cells that must be simulated is large and is typically constrained by computing limitations.

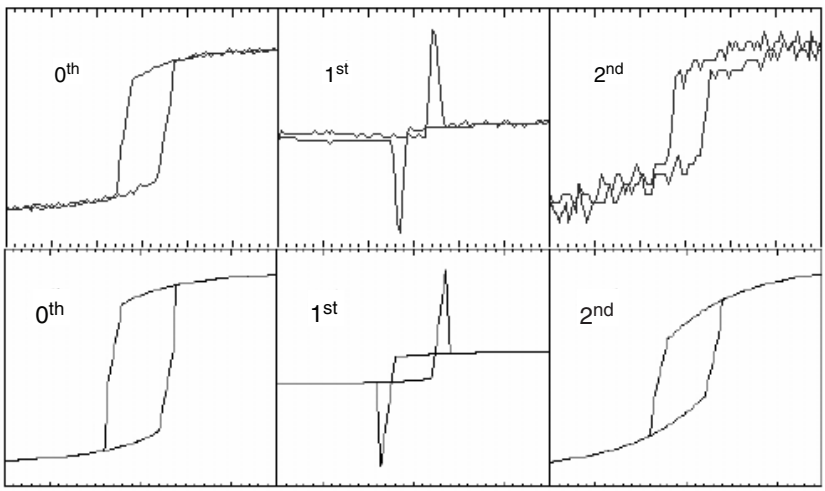

Figure 8. D-MOKE zeroth–second-order hysteresis loops for Py square rings with $H \parallel$ diagonal. The upper loops are experimental. The lower loops are calculated using micromagnetics from an asymmetric square ring.

5. Results

There are quite a large number of publications that have reported D-MOKE hysteresis loops [14, 17–35]. Here we will review only those articles in which information about magnetic domains has been extracted from diffracted hysteresis loops. Articles in which D-MOKE loops are shown but not interpreted are not individually addressed. For presentation purposes, the results are not discussed in chronological order.

It should be recalled that in comparing theory with experiment one must consider many sources for possible discrepancies. Experimental artefacts (some of the measured loops are very weak and noisy), intrinsic flaws in the assumptions made in deriving equation (5) used for the analysis and errors in the parameters (both magnetic material parameters and shape related issues) chosen for the micromagnetic simulations can all influence the comparison. In particular, we will show below that subtle shape changes can have profound effects on the micromagnetic simulations. As mentioned in the previous section, the theory that will be used for the interpretation of D-MOKE loops has evolved in time. Initially the theory considered only the real part of the form factor, and the domain structures within the particles were initially chosen *ad hoc* to produce agreement.

5.1. Magnetic gratings [20, 5, 7, 31, 32, 12]

Many of the first publications were performed on gratings [17, 18, 20–24] and dealt mainly with understanding the intensities of the magnetic signal in the saturated state: this aspect will not be reviewed here. In some of these investigations the shape of the loops during reversal was discussed [17, 18, 20, 21, 31]. In [17] it was concluded that the shapes reflected the domain formation via the spatial Fourier transform of the magnetization profile, i.e. the form factor. Although no specific domain structures were extracted, in [20, 5] and [7] it was shown that an *ad hoc* three-domain model provided a qualitative description of the D-MOKE loops. In [31] and [32] the longitudinal MOKE configuration was used to probe the gratings. In [12] the variation of the magnetization perpendicular to a grating was studied in various diffracted orders, from which a reversal via coherent rotation was deduced.

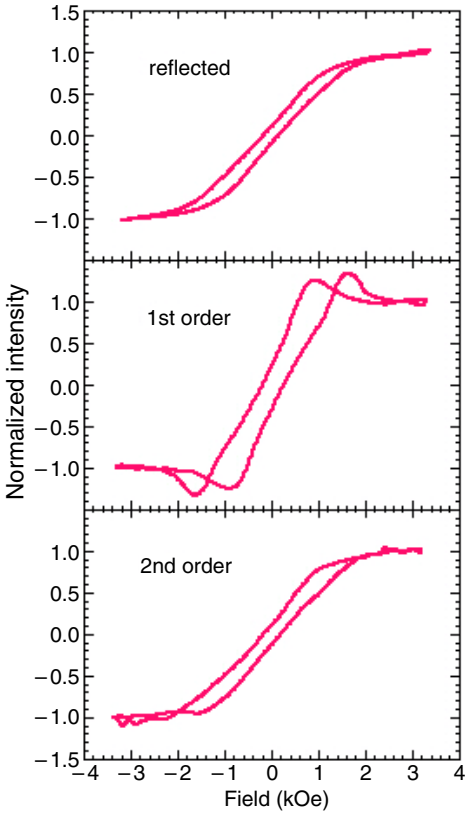

Figure 9. D-MOKE loops from a superlattice array of discs and ellipses.

5.2. Vortices in circular permalloy (Py) discs [14]

The measured hysteresis loops for various orders from an array of 800 nm Py discs, 60 nm thick, on a 1.6 μm square lattice are shown in figure 1. In figure 3 we show the zeroth–third-order magnetic form factors (equation (4)), calculated via micromagnetic simulations as described in the previous section. These form factors reflect the formation of a magnetic vortex in the discs. Using these form factors and equation (5), success in mimicking the measured loops by adjusting $A_n = -0.5n$ is achieved. The calculated loops are shown in figure 4; they must be compared with the experimental loops in figure 1. Qualitatively the shapes of the experimental loops are reproduced. The origins of the discrepancies are not yet understood although some simple possible reasons such as changes in A_n and/or errors in the reciprocal lattice vectors have been ruled out. The discrepancies could be due to: (a) not all particles in the array behave identically; (b) equations (4) and (5) do not provide a complete description; or (c) the parameters in the simulation are incorrect. The latter point could, in principle, be tested. However, the large number of parameters needed for the simulation make this a non-trivial exercise. For example one can change the value of M, introduce anisotropies (magnitude and direction), shape deviations, cell size in the simulation, interparticle coupling, convergence criteria, etc.

In [14], instead of attempting to refine the fits to the hysteresis loops, the authors concentrated on the more qualitative features. It was noticed that according to equation (5),

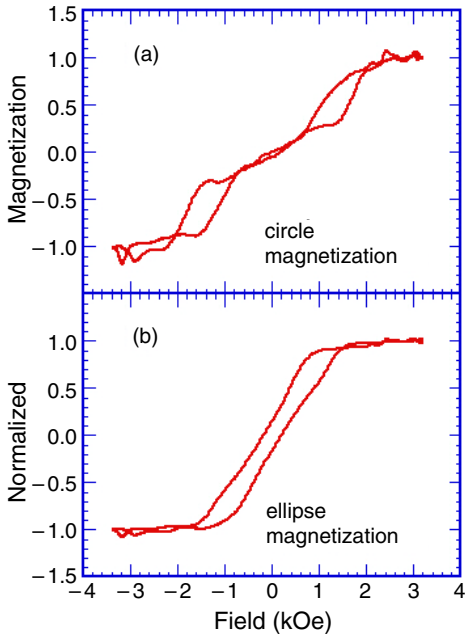

Figure 10. Hysteresis loops of the disc (a) and ellipse (b) sublattices extracted from the data in figure 9.

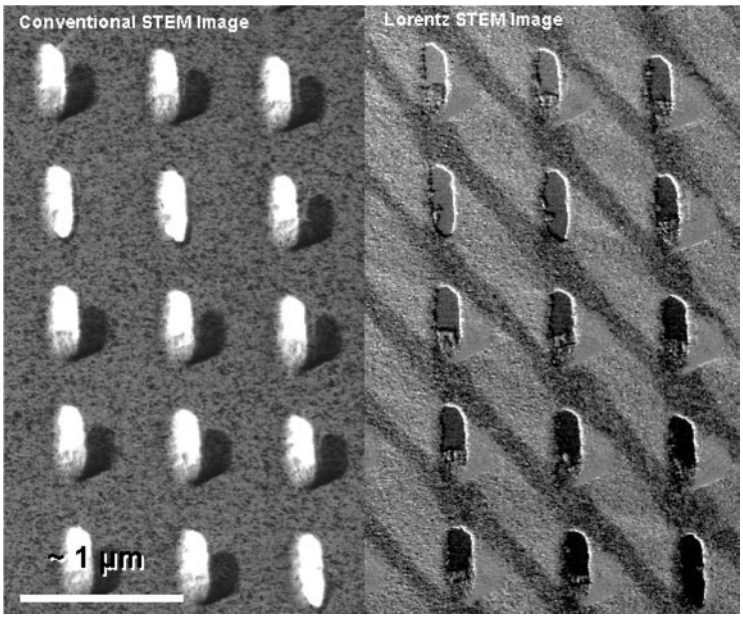

Figure 11. Left: an SEM image of an Fe film with elliptical holes. Right: a scanning Lorentz microscopy image of the same sample at remanence.

hysteresis loops on opposite sides of the reflected beam should be different because the sign of the imaginary part of the form factor is reversed when $n \rightarrow -n$. The experimental and

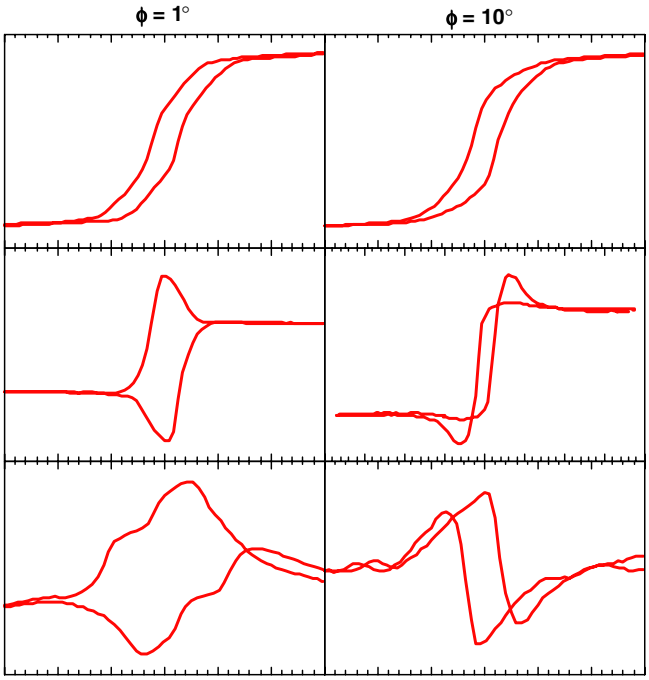

Figure 12. Zeroth- and first-order longitudinal and first-order transverse D-MOKE hysteresis loops for film with elliptical holes. (Note that 'longitudinal' and 'transverse' refer to the component of the magnetization, not the type of Kerr geometry.) The field was applied at 1° and 10° from the short ellipse axis in the left and right columns, respectively.

calculated ±second-order loops are compared in figure 5 and show not only that the asymmetry exists, but also that the theory accounts for it quite well.

Because the theoretical loops are obtained from the calculation on a single disc while the experimental data originate from thousands of discs, agreement between theory and experiment requires the vortex chirality to be identical in the great majority of discs. Since the two chiralities in a circular disc should be equivalent and hence the nucleation of + or − chirality should be random, this result was surprising. It was concluded that the coherent chirality in the array was due to small—visually unobservable—deviations from perfect circularity, and that these deviations were the same for all discs and were generated during the fabrication process. The left–right asymmetry of the discs (relative to the applied field) is the key factor that determines the chirality of the vortex state that nucleates during the reversal process. Shape induced preferential chirality has also been observed using Lorentz microscopy [36] in discs fabricated with a flat edge. This now makes it clear that it is possible to design particles explicitly to yield a chirality of choice.

5.3. Reversal in square Permalloy rings [34]

An SEM image of a Py ring array is shown in figure 6. The rings are 25 nm thick, the ring widths are 240 nm and the length of each side of a ring is 2.1 μm. The zeroth–second-order hysteresis loops measured with the field along the edge and along the diagonal are shown in the upper halves of figures 7 and 8 respectively. The zeroth-order loops (equivalent to a conventional magnetization loop) for both field directions are consistent with the magnetization of each edge aligning parallel to the edge at zero field leading to remanant magnetizations of 0.5 and

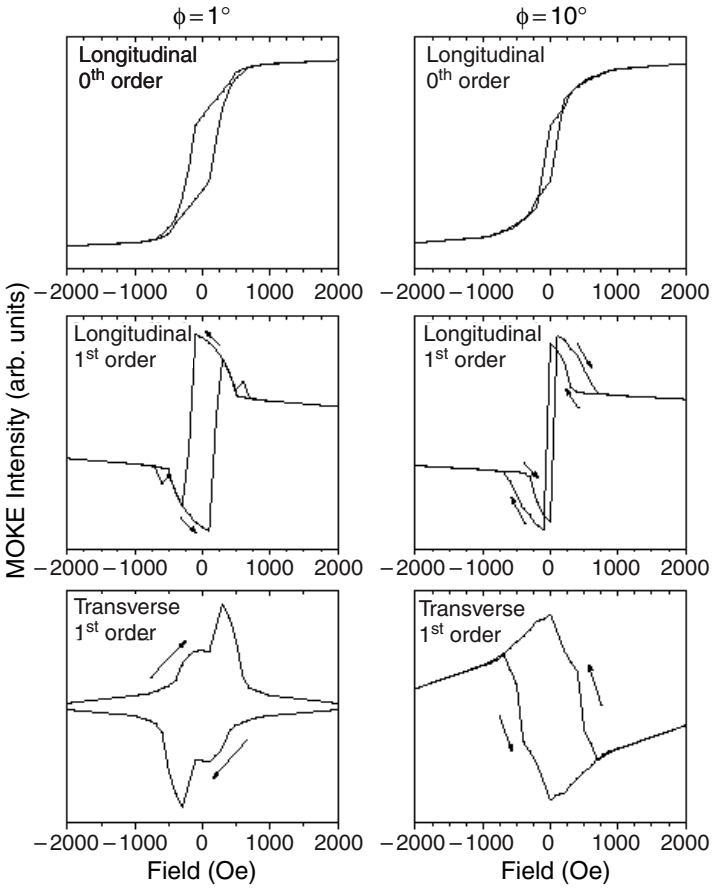

Figure 13. Calculated hysteresis loops for the case described in figure 12.

0.75 for the two field directions. This is also consistent with the results of micromagnetic simulations of the ring. However, because the simulations of a square ring did not reproduce the experimentally observed sharp spikes in the first-order loops, it was necessary to search for the origin of this qualitative discrepancy.

Agreement between micromagnetic simulations and experiment was finally achieved by making the widths of two opposite arms of the ring in the simulations different. This symmetry breaking change to the ring leads to one arm switching earlier than the other. In turn this leads to a large imaginary component of the form factor and leads to the hysteresis loops shown in the lower halves of figures 7 and 8. For the field along the diagonal (figure 8) the agreement is good for all orders (out to order 6 not shown here). For the field along the edge good agreement is obtained for the zeroth- and first-order loops but not for the second-order loop. (Also not shown here is that the agreement is marginal for the third and fourth orders and good for all other orders out to the eleventh.) It is assumed that the discrepancies in the second–fourth orders are due to the neglect of some, as yet unidentified, feature of the rings.

The asymmetric switching of opposing ring edges leads to the creation of intermediate, metastable states during reversal. Using the D-MOKE technique it was possible to trap the system in these states and then observe them using magnetic force microscopy (MFM), again providing confidence in the theoretical formalism developed to interpret D-MOKE loops.

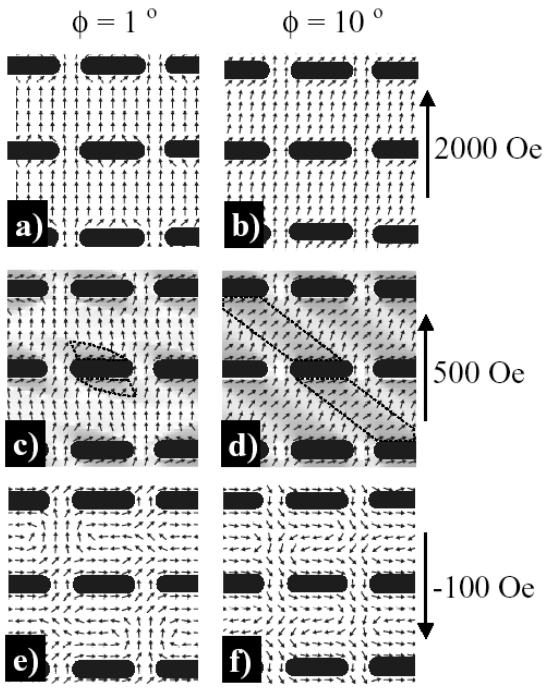

Figure 14. Magnetic configurations obtained in the micromagnetic simulations that led to figure 12. For the same applied field strength the spin distribution depends very strongly on the field direction. Note in particular that in (e) and (f) at −100 Oe, the vertical 'channels' are reversed in one case but not the other.

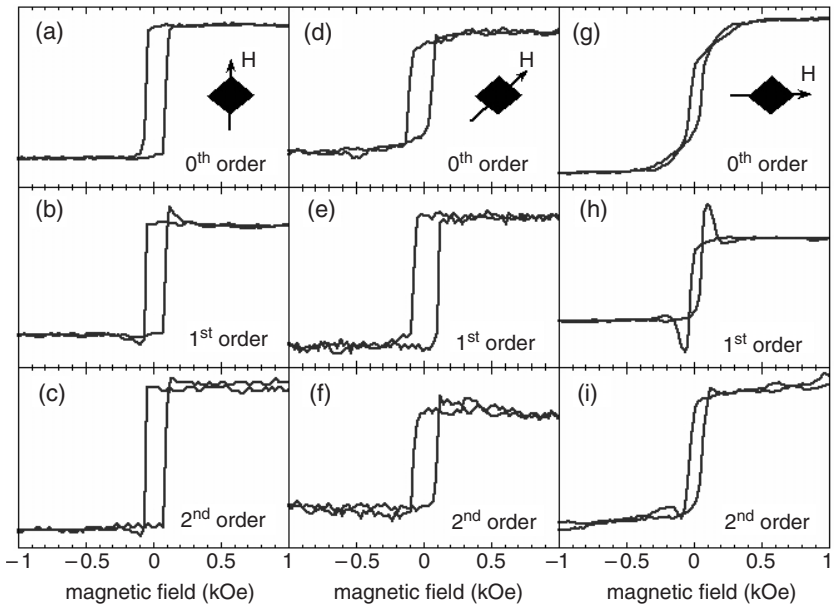

Figure 15. Experimental D-MOKE loops for small squares for various orders and directions of the applied field.

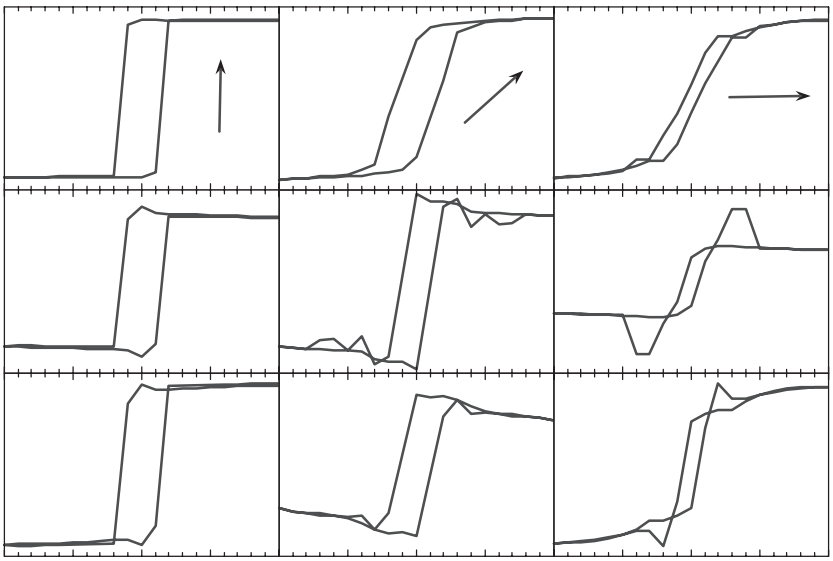

Figure 16. Micromagnetically simulated loops for the sample investigated in figure 15. The difference between the loops for the field along the two diagonals was accounted for by an in-plane anisotropy.

5.4. Superlattice dot arrays [26]

The D-MOKE technique was also used to investigate a superlattice array of discs and ellipses. At the time the work was done the theoretical formalism had not been developed. Nonetheless, noting the even and odd diffraction orders produced differently shaped loops, shown in figure 9, the researchers interpreted their data as the in-phase and out-of-phase contributions from the discs and ellipses. (The same conclusion can be reached using the form factor approach where the integration in equation (4) must now be carried out over the two magnetic particles in the unit cell.) Although no attempt was made to extract the magnetization profile within each magnetic element, they did extract the hysteresis loops of the two individual constituents, discs and ellipses, which are shown in figure 10.

5.5. An array of circular holes in an Fe film [25]

The work [25] reported the diffracted hysteresis loops from a 40 nm thick Fe film with 200 nm circular holes on a 2 μm square lattice. In that article the mathematical expression for the magnetic form factor was introduced but the results were interpreted prior to the introduction of micromagnetic simulations into the analysis. Two items however are worthy of mention: the authors did experimentally verify that the diffracted intensities (i.e. the non-magnetic part) are correctly described by the first term in equation (3) and that the peaks observed in the first-order D-MOKE loops could be explained by the formation of 'blade' domains which form during reversal around each hole.

5.6. An array of elliptical holes in an Fe film [27, 33]

An SEM image of the array of elliptical holes in an Fe film studied in the investigations [27, 33] is shown on the left of figure 11. The Fe film is 60 nm thick and the 200×800 nm elliptical holes are on a 1×1 μm square lattice. The D-MOKE technique was used to investigate the switching

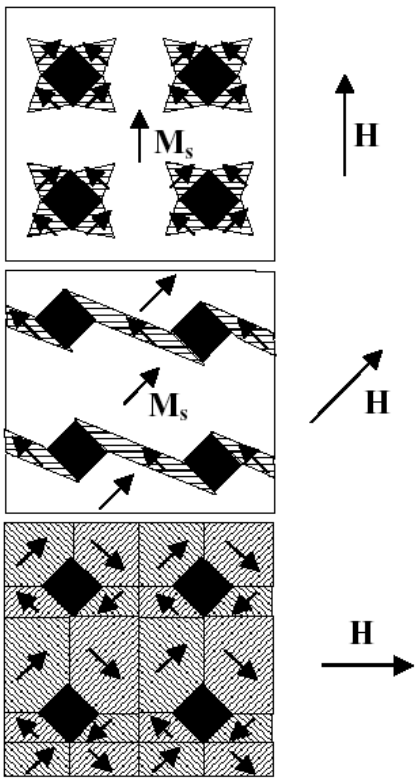

Figure 17. A schematic diagram of domains appearing in a film with square holes for different directions of the applied field. The unpatterned film has a horizontal hard axis.

mechanism for different directions of the applied field. Figure 12 shows the D-MOKE loops measured for two directions of the applied field: 1° and 10° from the short ellipse axis. Because the zeroth-order longitudinal loops are quite similar for the two directions of the field, it would be tempting to conclude that the switching mechanisms are also similar. However, the first-order longitudinal and transverse (the transverse component of the magnetization) loops are indicative that the domain formation during reversal is quite different. The corresponding calculated loops are shown in figure 13 and it can be see that they capture the essential features of the experimental ones. This agreement in turn enables the spin configurations in the micromagnetic simulations to be interpreted with some confidence. In figure 14 we show the spin configurations at three different field values for the two directions. (These images correspond to the centre region of a 5×5 unit cell micromagnetic simulation area.) It can be seen that while the spin configurations are similar at high fields, they differ dramatically during reversal. Particularly striking is that at -100 Oe the vertical channels are reversed for one field direction but not for the other.

5.7. An array of square holes in an Fe film [30]

A D-MOKE study of an array of square holes on a square lattice in an Fe film yielded the loops shown in figure 15. The direction of the applied field is also indicated in the figures. The most surprising feature of the data in this figure is that the loops for the two 'equivalent' diagonal directions produce inequivalent loops. In this case the explanation turned out not

to be related to subtle shape effects of the holes or the lattice but to a growth induced anisotropy in the Fe film itself. (This anisotropy was detected using Brillouin scattering.) Including the anisotropy in the micromagnetic simulations led to the hysteresis loops shown in figure 16 that, qualitatively, reproduce the measured loops. Schematically, the domain configurations exhibited by micromagnetic simulations at remanence are shown in figure 17. In all cases domain formation is driven by the 'magnetic charges' at the hole boundaries. The different domain shapes are determined by the subtle interplay between the domain wall and the anisotropy energies.

6. Discussion and comparison with other techniques

The examples presented in the previous section show that the D-MOKE technique is one that can yield information on the magnetic spin distribution in nanometre-sized particles. With the aid of micromagnetic simulations it has enabled the detection of coherent chirality of vortices in circular discs, unexpected metastable states during reversal of square rings, hysteresis loops of the two constituents of a superlattice array, the formation of blade domains in an array of circular holes and the changes in reversal path as a function of the direction of the applied field.

On the basis of the information that can be extracted, the D-MOKE technique must compared with other techniques that yield similar information; the most common of these are: (i) micromagnetic simulations; (ii) magnetic force microscopy (MFM); and (iii) Lorentz scanning transmission electron microscopy. Other techniques are being developed (e.g. x-ray photoemission electron microscopy (PEEM)) but for many it is still too early to evaluate all their strengths and limitations.

Advantages	Disadvantages
The D-MOKE technique	
No special sample preparation	Requires an array ($\lambda/2 <$ period $\lesssim 10\lambda$)
Provides information at all fields	Measures many elements
Versatile (temperature, orientation)	Needs simultaneous micromagnetic simulations
Micromagnetic simulations	
Can tackle any problem (computer limited)	Requires all the correct input parameters
Provides information at all fields	Not easy to include interparticle coupling
MFM	
No special sample preparation	Images of 'domains' not easy to interpret
Can view single element	In-field measurements are non-trivial
LSTEM	
Can view single particle	Requires substrate transparent to electrons
Provides complete magnetic configuration	In-field measurements are non-trivial

The above simplistic evaluation of the techniques available for studying magnetization in submicron-sized particles, rather than highlighting the superiority of any single technique, emphasizes that they are most powerful when used in consort rather than as alternatives. Perhaps the most important role that will be played by the D-MOKE technique in the future is in providing data against which micromagnetic simulations can be tested. Conversely, when micromagnetic simulations do reproduce the D-MOKE results, all the other predictions from them can be accepted with considerably more confidence.

In general, however, the recent achievements in the field of nanomagnetism are, to a great extent, due to the skill with which all of the above techniques are being jointly and systematically applied to this relatively new field.

Acknowledgments

Work at ANL was supported by the US Department of Energy, BES Materials Sciences, under Contract W-31-109-ENG-38. PV gratefully acknowledges financial support from the MURST-COFIN 2003 research programme.

References

[1] Moog E R and Bader S 1985 *Superlatt. Microstruct.* **1** 543
Bader S D, Moog E R and Grünberg P 1986 *J. Magn. Magn. Mater.* **53** L295
[2] Zak J, Moog E R, Liu C and Bader S D 1990 *J. Magn. Magn. Mater.* **89** 107
[3] Qui Z Q and Bader S D 2000 *Rev. Sci. Instrum.* **71** 1243
[4] van Labeke D, Vial A, Novosad V, Souche Y, Schlenker M and Dos Santos A D 1996 *Opt. Commun.* **124** 519
[5] Vial A and van Labeke D 1998 *Opt. Commun.* **153** 125
[6] Stashkevich A A 2000 *Opt. Commun.* **178** 1
[7] Pagani Y, van Labeke D, Guizal B, Vial A and Baida F 2002 *Opt. Commun.* **209** 237
[8] Ciprian D and Pistora J 2001 *Acta Phys. Pol.* A **99** 33
[9] Maystre D 1984 *Progress in Optics* vol XXI, ed E Wolf (Amsterdam: Elsevier Science BV) p 1
[10] Suzuki Y, Chappert C, Bruno P and Veillet P 1997 *J. Magn. Magn. Mater.* **165** 516
[11] Garcia-Mochales P, Costa-Krämer J, Armelles G, Briones F, Jaque D, Martin J and Vicent J 2002 *Appl. Phys. Lett.* **81** 3206
[12] Costa-Krämer J, Guerrero C, Melle S, Garcia-Mochales P and Briones F 2003 *Nanotechnology* **14** 239
[13] Azzam R M and Bashara N M 1972 *Phys. Rev.* B **5** 4721
[14] Grimsditch M, Vavassori P, Novosad V, Metlushko V, Shima H, Otani Y and Fukamichi K 2002 *Phys. Rev.* B **65** 172419
[15] Brown W F Jr 1978 *Micromagnetics* (New York: Krieger)
[16] Donahue M and Porter D 2000 *OOMMF User's Guide, Version 1.0. Interagency Report* NISTIR 6376 (Gaithersburg, MD: National Institute of Standards and Technology)
[17] Geoffroy O, Givord D, Otani Y, Pannetier B, Dos Santos A D, Schlenker M and Souche Y 1993 *J. Magn. Magn. Mater.* **121** 516
[18] Souche Y, Schlenker M and Dos Santos A D 1995 *J. Magn. Magn. Mater.* **140–144** 2179
[19] Bardou N, Bartenlian B, Rousseaux F, Decanini D, Carcenac F, Chappert C, Veillet P, Beauvillain P, Megy R, Suzuki Y and Ferre J 1995 *J. Magn. Magn. Mater.* **148** 293
[20] Souche Y, Geoffroy O, Novosad V, Pishko V and Pannetier B 1996 *Proc. Magneto-Optical Recording Int. Symp.*; *J. Mag. Soc. Japan* **20** (Suppl. S1) 393
[21] Gadetsky S, Syrgabaev I, Erwin J and Mansuripur M 1996 *J. Opt. Soc. Am.* A **13** 314
[22] Eremenko V, Novosad V, Pishko V, Geoffroy O, Souche Y and Pannetier B 1997 *JETP Lett.* **66** 495
[23] Souche Y, Novosad V, Pannetier B and Geoffroy O 1998 *J. Magn. Magn. Mater.* **177–181** 1277
[24] Novosad V, Souche Y, Pishko V, Crozes T, Otani Y and Fukamichi K 1999 *IEEE Trans. Magn.* **35** 3145
[25] Vavassori P, Metlushko V, Osgood R III, Grimsditch M, Welp U, Crabtree G, Fan W, Brueck S R, Ilic B and Hesketh P 1999 *Phys. Rev.* B **59** 6337
[26] Vavassori P, Metlushko V, Grimsditch M, Ilic B, Neuzil P and Kumar R 2000 *Phys. Rev.* B **61** 5895
[27] Guedes I, Zaluzec N, Grimsditch M, Metlushko V, Vavassori P, Ilic B, Neuzil P and Kumar R 2000 *Phys. Rev.* B **62** 11719
[28] Grimsditch M, Guedes I, Vavassori P, Metlushko V, Ilic B, Neuzil P and Kumar R 2001 *J. Appl. Phys.* **89** 7096

[29] Shen Y T, Wu Y H, Chong T C, Xie H, Guo Z B, Li K B and Qiu J J 2001 *Appl. Phys. Lett.* **79** 2034
[30] Guedes I, Grimsditch M, Metlushko V, Vavassori P, Camley R, Ilic B, Neuzil P and Kumar R 2002 *Phys. Rev.* B **66** 014434
[31] Schmitte T, Westerholt K and Zabel H 2002 *J. Appl. Phys.* **92** 4524
[32] Schmitte T, Schwöbken O, Goek S, Westerholt K and Zabel H 2002 *J. Magn. Magn. Mater.* **240** 24
[33] Guedes I, Grimsditch M, Metlushko V, Vavassori P, Camley R, Ilic B, Neuzil P and Kumar R 2003 *Phys. Rev.* B **67** 024428
[34] Vavassori P, Grimsditch M, Novosad V, Metlushko V and Ilic B 2003 *Phys. Rev.* B **67** 134429
[35] Lazarenko S, Kirilyuk A, Rasing Th and Lodder J 2003 *J. Appl. Phys.* **93** 7903
[36] Schneider M, Hoffmann H and Zweck J 2001 *Appl. Phys. Lett.* **79** 3113